Reprinted from

THEORETICAL AND APPLIED MECHANICS

Volume 37

Proceedings of the 37th Japan National Congress for Applied Mechanics, 1987

Edited by Japan National Committee for Theoretical and Applied Mechanics Science Council of Japan

UNIVERSITY OF TOKYO PRESS, 1989

Numerical Simulation of Flow Ejected from a Nozzle by Electric Force

Yusuke TAKEDA,* Daisuke TAKAHASHI,[2]* Katsuya ISHII,[3]* and Hideo TAKAMI[2]*

* *Imaging Technology Research Center, Ricoh Company Limited, Tokyo,* [2]* *Department of Applied Physics, University of Tokyo, Tokyo,* [3]* *Institute of Computational Fluid Dynamics, Tokyo*

A numerical method that makes use of equations of incompressible flow with a free surface and an electric field equation is discussed and applied to the study of a flow ejected from a nozzle by electrostatic force.

In this study, the fluid is treated as electrically perfect conductor. The improved marker and cell method[6] and charge simulation method[7] are used to solve the motion of fluid and electric field, respectively. The surface configuration is determined by the balance between the surface tension of the fluid and electrostatic force.

Calculations are performed for several variations of fluid characteristics, strength of the electric field, and nozzle dimension. Computational results are reasonable for each variable.

I. INTRODUCTION

It is a very important and interesting problem to form small liquid droplets in combustion or ink jet technology. Typical methods apply a pressure pulse or electrostatic force to fluid in a nozzle. Numerical simulations of such flow using axisymmetrical Navier-Stokes equation have been reported.[1–3] For ink jets, some experimental or analytical studies of fluid deformation by electrostatic force have been performed.[4,5] However, few numerical studies of this phenomenon have been carried out because it is difficult to determine the surface configuration by taking account of both surface tension of the fluid and the electrostatic force. Therefore, quantitative evaluation of the contribution of variables in this phenomenon (surface tension of the fluid, kinematic viscosity, nozzle dimension, etc.) to deformation has not yet been performed.

In this paper, we calculate the axisymmetrical Navier-Stokes equation and the axisymmetrical Laplace equation which govern the motion of the fluid and the electric field, respectively. Here, in order to simplify the calculation, we assume that the fluid is an electrically perfect conductor. We use the improved marker and cell method[6] for the fluid motion and use the charge simulation method[7] for the electric field which can treat the surface configuration more easily than the finite difference or finite element method. At each time step, the Navier-Stokes equation is integrated and the Poisson equation for pressure is solved iteratively using the boundary condition at the free surface which determines the surface tension of the fluid and the electrostatic force.

Computations are performed for several combinations of surface tension of the fluid, kinematic viscosity of the fluid, length of the nozzle, radius of the nozzle, and strength of the electric field.

II. BASIC EQUATIONS

The governing equations that describe the motion of the fluid are the equation of continuity and the Navier-Stokes equation. In an axisymmetric coordinate system (z, r), they are expressed in the following forms:

$$\frac{\partial u}{\partial z} + \frac{\partial v}{\partial r} + \frac{v}{r} = 0, \tag{1}$$

$$\frac{\partial u}{\partial t} + (\boldsymbol{u} \cdot \nabla) u = -\frac{\partial p}{\partial z} + \nu \Delta u, \tag{2}$$

$$\frac{\partial v}{\partial t} + (\boldsymbol{u} \cdot \nabla) v = -\frac{\partial p}{\partial r} + \nu\left(\Delta v - \frac{v}{r^2}\right), \tag{3}$$

where (u, v) are (z, r) components of the velocity, p the pressure, and ν the kinematic viscosity. By taking the divergence of the Navier-Stokes equation, we get the Poisson equation for the pressure:

$$\Delta p = -\frac{\partial D}{\partial t} + \nu \nabla D - \Delta \cdot ((\boldsymbol{u} \cdot \nabla)\boldsymbol{u}), \tag{4}$$

$$D = \nabla \cdot \boldsymbol{u}. \tag{5}$$

The governing equation of the electric field is the Laplace equation:

$$\Delta \phi = 0 \tag{6}$$

where ϕ is the electric potential.

III. BOUNDARY CONDITIONS

The boundary conditions are as follows:

1) On the wall of the nozzle, we impose no-slip condition for velocity:

$$u = 0, \qquad v = 0. \tag{7}$$

The pressure on the wall is derived from the Navier-Stokes equations.

2) At the entrance of the nozzle, the velocity is determined by extrapolation and the pressure is assumed to be constant with its value p_0 determined by

$$p_0 = \frac{2\gamma}{R_0} \tag{8}$$

where γ is the surface tension of the fluid, and R_0 the radius of the nozzle.

3) On the free surface, we impose the condition of continuity of stress. If we neglect the effect of the external fluid (air), this condition is expressed as

$$\sigma^*_{i,j} \cdot n_j = \sigma^+_{i,j} \cdot n_j \tag{9}$$

where $\sigma^*_{i,j}$ and $\sigma^+_{i,j}$ are fluid and electric stress tensor, respectively, and n_j the normal vector to the surface. Each stress tensor is expressed as follows:

$$\sigma^{*}_{i,j} = -p_s \delta_{i,j} - \gamma\left(\frac{1}{R_1} + \frac{1}{R_2}\right)\delta_{i,j} + \nu\left(\frac{\partial u_i}{\partial x_j} + \frac{\partial u_j}{\partial x_i}\right), \tag{10}$$

$$\sigma^{+}_{i,j} = D_i \cdot E_j - \frac{1}{2} D_k E_k \sigma_{i,j} \tag{11}$$

where $\delta_{i,j}$ is Kronecker's delta, D_i the electric flux, and R_1 and R_2 the principal radii of curvature of the surface. Here, we neglect the viscous term in Eq. (10) to simplify the calculation. Finally, the surface pressure p_s is given by the following equation:

$$p_s = -\gamma\left(\frac{1}{R_1} + \frac{1}{R_2}\right) + \frac{1}{2}\varepsilon E^2. \tag{12}$$

The velocity on the free surface is determined by extrapolation from the velocity inside the fluid.

IV. NUMERICAL METHOD

The improved marker and cell method was described in detail by Takahashi et al.[6] so that only a brief discussion of the basic features will be presented here. In the finite difference calculation, the Navier-Stokes equation (Eqs. (2) and (3)) and the Poisson equation for pressure (Eq. (4)) are approximated as follows:

$$u^{n+1} = u^n + \Delta t\left[-(\boldsymbol{u}^n \cdot \nabla)u^n - \left(\frac{\partial p}{\partial z}\right)^n + \nu \Delta u^{n+1}\right], \tag{13}$$

$$v^{n+1} = v^n + \Delta t\left[-(\boldsymbol{u}^n \cdot \nabla)v^n - \left(\frac{\partial p}{\partial r}\right)^n + \nu\left(\Delta v^{n+1} - \frac{v^{n+1}}{r^2}\right)\right], \tag{14}$$

$$\Delta p^n = -\frac{D^n}{\Delta t} - \nabla \cdot ((\boldsymbol{u}^n \cdot \nabla)\boldsymbol{u}^n) \tag{15}$$

where Δt is the interval of time difference and the index n denotes the number of the time step. These equations are calculated in the form of the central difference. A unit of rectangular mesh (which we call "cell") is classified into empty (E), fluid (F), surface (S), or wall (W) cell. The physical quantities of fluid (velocity and pressure) are represented in the center of each cell. Markers are put only in S cells and moved with the velocity of S cells. The typical classification of the cells and the arrangement of the markers are shown in Fig. 1. The stress due to surface tension at the surface cell is calculated from the principal radii of surface curvature that are determined from the positions of markers. Markers are rearranged at each time step and the number of markers in each cell is always controlled to be constant. Using Eq. (15), pressure at F cells is calculated iteratively with the boundary condition of the pressure of S cells. Using Eqs. (13) and (14), velocity at F cells is integrated by an iterative method and the velocity of S cells is determined by extrapolation.

As regards calculations of electric field, we use the charge simulation method.[7] Since the fluid is an electrically perfect conductor, we only consider the nonfluid region. In this calculation, the electric potential on the surface of the fluid and the nozzle is 0 and the potential at the electrode is V. We choose typical points (equipotential points) on the free surface of the fluid, the nozzle surface, and the electrode. Moreover, we put ring-shaped virtual charges inside the fluid, the nozzle, and the electrode. Figure 2 shows the typical

arrangement of equipotential and virtual charge points. The charge at each virtual charge point Q_j is calculated by solving the following equation:

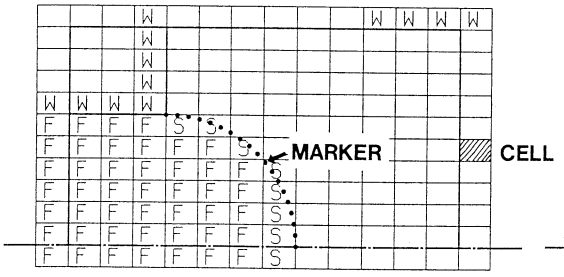

Fig. 1. Typical classification and arrangement of markers. F: Fluid cell; S: surface cell; W: wall cell; □: empty cell.

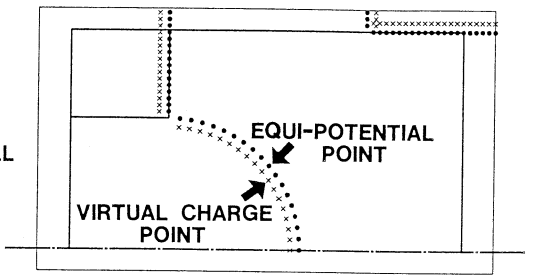

Fig. 2. Typical arrangement of equipotential and virtual charge points.

$$\sum_{j=1}^{m} P_{i,j} \cdot Q_j = \begin{cases} 0 \text{ (on the fluid or nozzle)} \\ V \text{ (on the electrode)} \end{cases} \quad (i = 1, 2, \ldots, m) \tag{16}$$

where m is the number of equipotential points and the coefficient $P_{i,j}$ is the electric potential at the i-th position induced by a unit charge at the j-th position. After solving Eq. (16), the electric potential at the equipotential point ϕ_i is calculated by

$$\phi_i = \sum_{j=1}^{m} P_{i,j} \cdot Q_j. \tag{17}$$

Electric field $\boldsymbol{E}_i$ is given by

$$\boldsymbol{E}_i = \sum_{j=1}^{m} \boldsymbol{F}_{i,j} \cdot Q_j \tag{18}$$

where the coefficient $\boldsymbol{F}_{i,j}$ is the electric field at the i-th position by a unit charge at the j-th position.

Finally, the computation procedure is as follows:

1) At the n-th time step, markers are placed as they approximate the configuration of the fluid region.

2) The values of stress due to the surface tension of S cells are calculated from the principal radii of curvature.

3) Using Eqs. (16)–(18), the values of electrostatic force of S cells are calculated.

4) The values of pressure of S cells are determined by Eq. (12).

5) Using Eq. (15), the values of pressure of F cells at the n-th time step are calculated by an iterative method.

6) Using Eqs. (13) and (14), the values of velocity of F cells at the $(n+1)$st time step are calculated by an iterative method.

7) Markers are moved with these velocities by time interval Δt.

8) The configuration of the fluid region at the $(n+1)$st time step is determined by the positions of markers and every cell is newly classified.

9) Return to step 2.

V. NUMERICAL RESULTS AND DISCUSSION

Figure 3 is a schematic illustration with the parameters used in the calculation. Initially, the surface configuration of the fluid is a half-sphere without electric field. In this situation, the fluid does not move since the surface stress of the fluid is equal to the pressure at the entrance of the nozzle. At $t=0$, an electric field is suddenly applied and the fluid begins to move. We calculate 6 cases with the scheme mentioned in Section 4. The condition in each case is shown in Table 1. Here, we regard case 1 as the standard case. Kinematic viscosity of the fluid (ν), surface tension of the fluid (γ), electric potential of the electrode (V) length of the nozzle (Ln), and the radius of the nozzle (R_0) used in case 1 are changed in case 2—case 6, respectively.

Figures 4–9 show the numerical results of each case. In these figures, velocity vectors

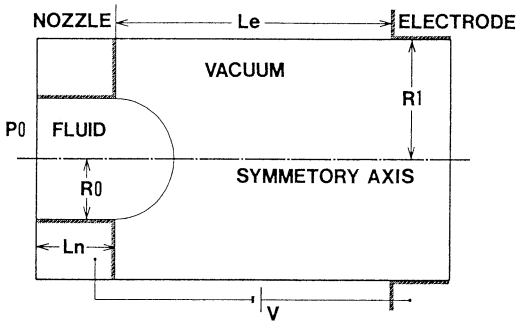

Fig. 3. Schematic illustration and parameters.

Table 1. Characteristics in cases 1–6.

Characteristics	Case 1	Case 2	Case 3	Case 4	Case 5	Case 6
Surface tension (dyn/cm)	25.0	25.0	15.0	25.0	25.0	25.0
Kinematic viscosity (cm^2/sec)	0.02	0.04	0.02	0.02	0.02	0.02
Electrode potential (V)	2000	2000	2000	4000	2000	2000
Nozzle radius ($\times 10^{-3}$mm)	100	100	100	100	100	150
Electrode radius (mm)	0.35	0.35	0.35	0.35	0.35	0.35
Nozzle length (mm)	0.2	0.2	0.2	0.2	1.2	0.2
Distance from nozzle exit to electrode (mm)	1.3	1.3	1.3	1.3	1.3	1.3
Pressure at entrance of nozzle (dyn/cm^2)	5000	5000	3000	5000	5000	5000
Mesh points (z)	200	200	200	200	300	200
Mesh points (r)	70	70	70	70	70	70
Mesh interval (z) (mm)	0.01	0.01	0.01	0.01	0.01	0.01
Mesh interval (r) (mm)	0.005	0.005	0.005	0.005	0.005	0.005
Time interval ($\times 10^{-6}$ sec)	0.75	0.75	0.75	0.75	0.75	0.75

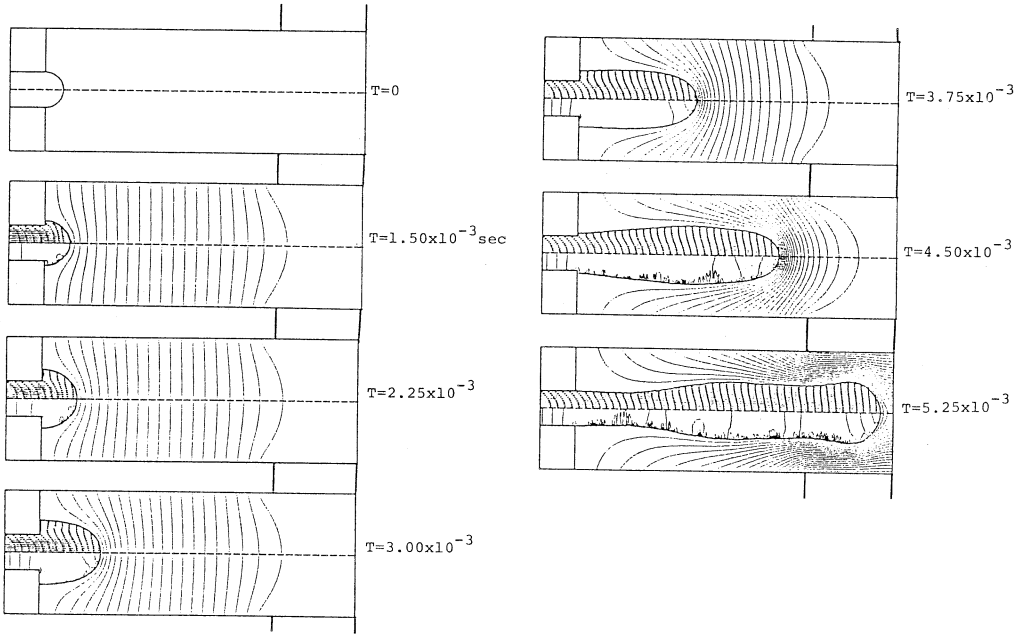

Fig. 4. Numerical results of case 1.

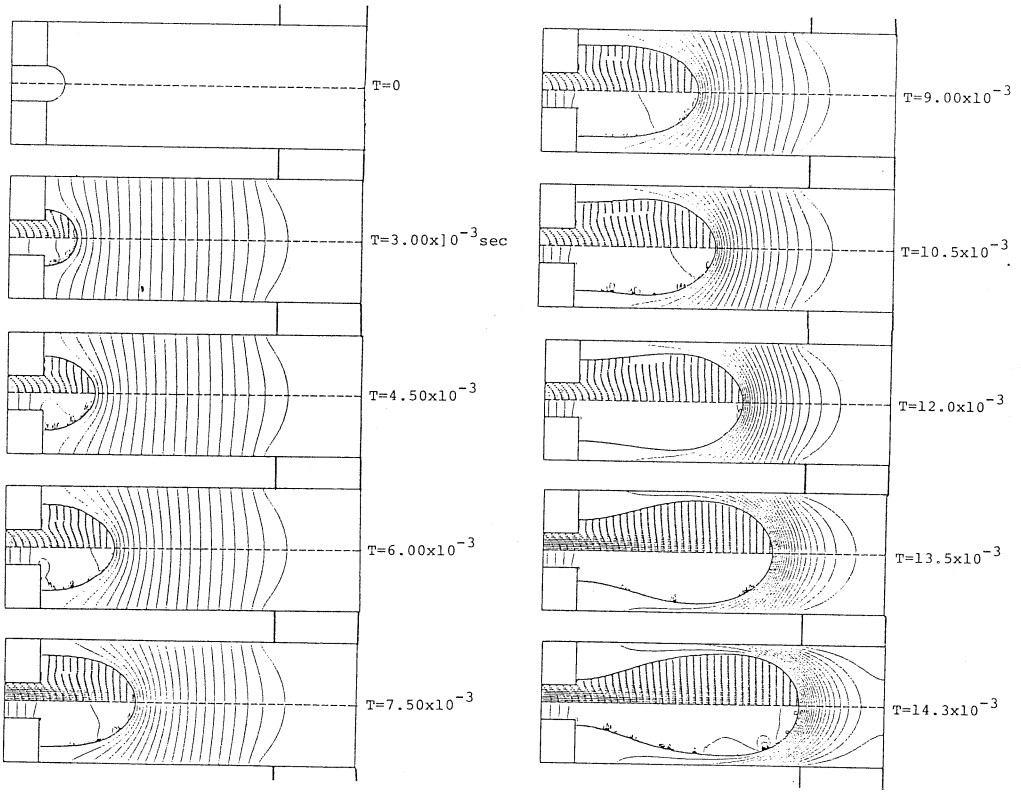

Fig. 5. Numerical results of case 2.

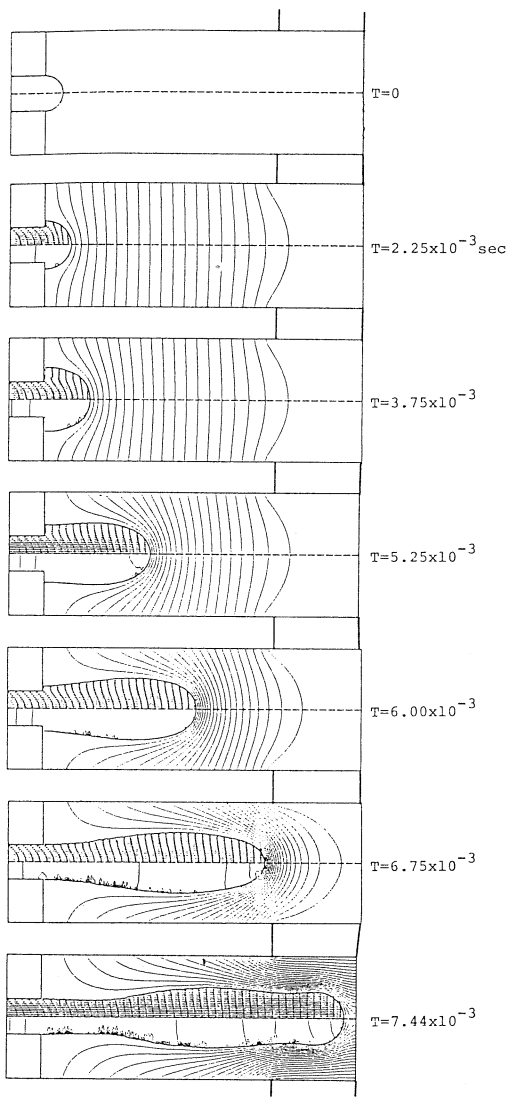

Fig. 6. Numerical results of case 3.

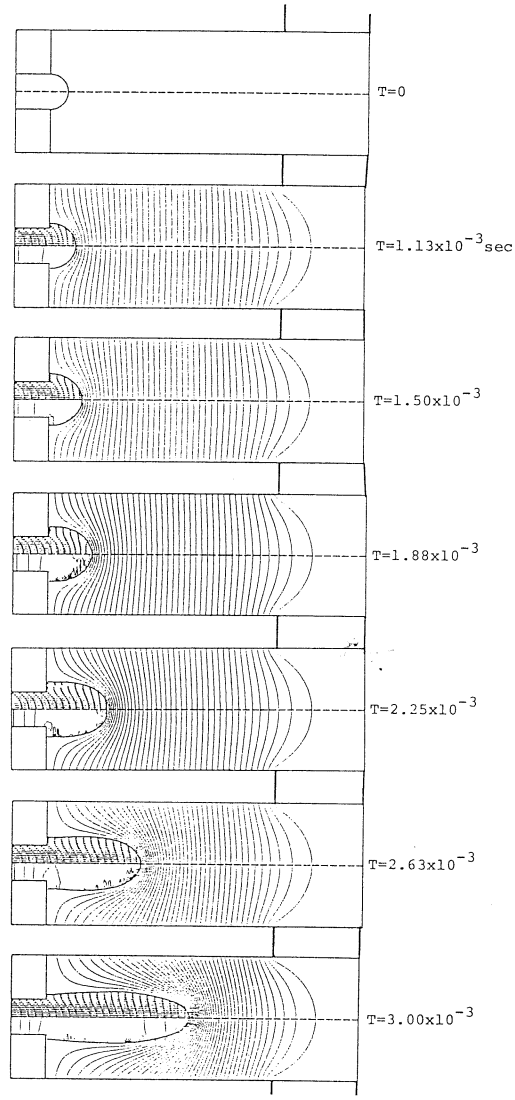

Fig. 7. Numerical results of case 4.

and pressure contours are plotted on, respectively, the upper and lower side of the symmetry axis in the fluid region and the contours of electric potential are plotted on the non-fluid region. Furthermore, Fig. 10 shows the relationship between time and the distance from the exit of the nozzle to the head of the jet. In Fig. 4, when the electric field is applied, the fluid is pulled in the z-direction expanding in the r-direction along the surface of the nozzle. Subsequently the electric field concentrates at the head of the jet and the z-component of velocity near the axis increases. Consequently, the fluid pulled out in the z-direction passes through the hole of the electrode without separating into droplets. In the case of larger kinematic viscosity (case 2), deformation speed of the fluid is slower than that in case 1. The fluid configuration is thicker in comparison with that in case 1. It is suspected,

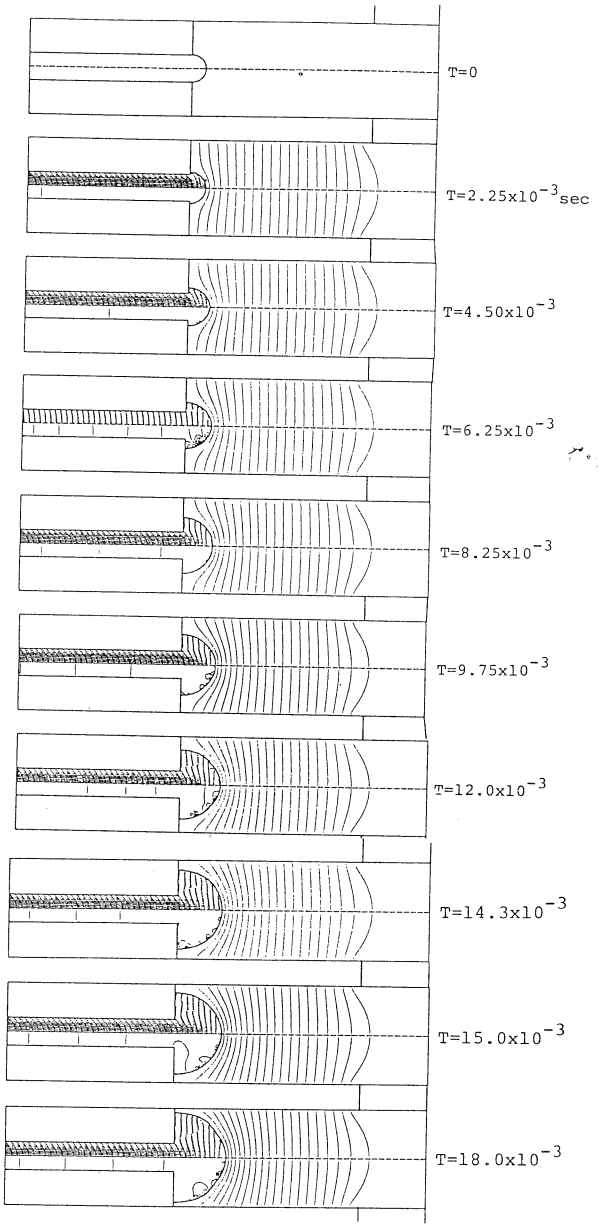

Fig. 8. Numerical results of case 5.

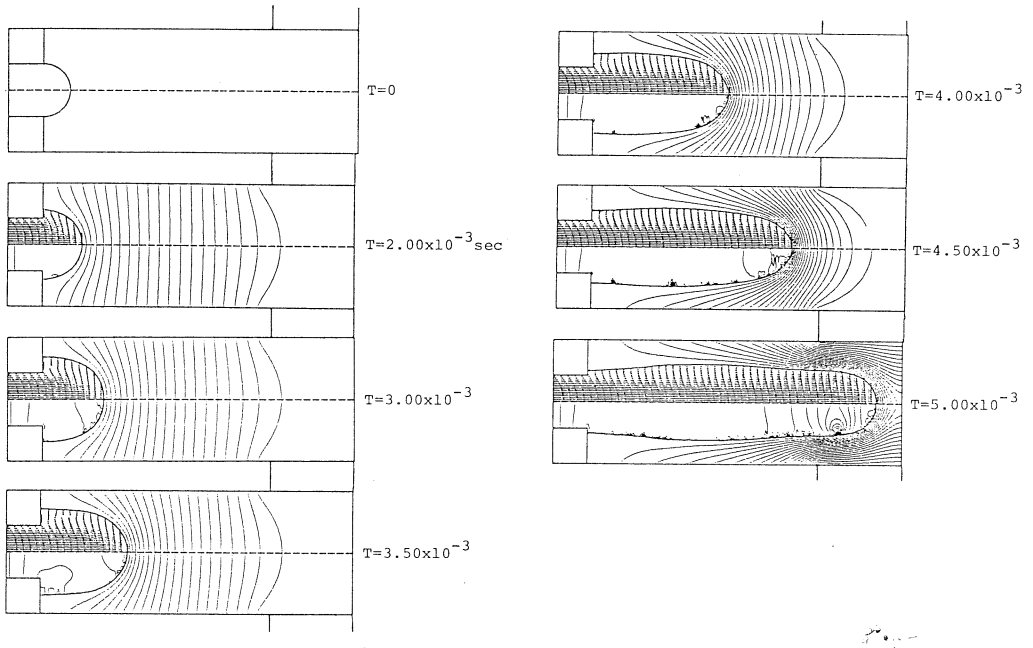

Fig. 9. Numerical results of case 6.

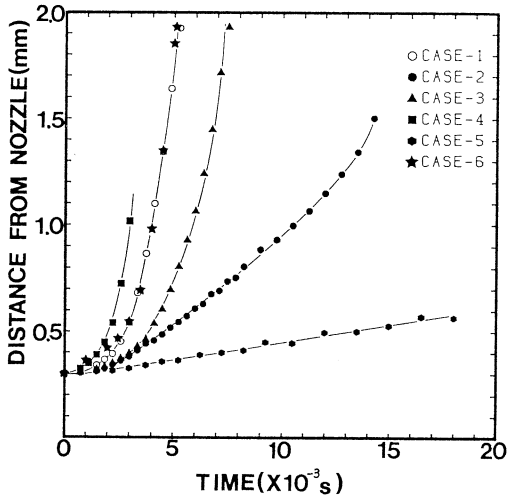

Fig. 10. Relationship between time and distance from nozzle exit to head of jet.

that these differences are caused by the pressure gradient in the nozzle which is proportional to the kinematic viscosity. In the case of smaller surface tension (case 3), the fluid configuration is much the same as that in case 1. However, deformation speed is lower than that in case 1 since the pressure at the entrance of the nozzle is smaller than that in case 1. In case 4, with stronger electric field, moving speed of the fluid is higher than in case 1, as expected. Moreover, the fluid configuration is sharpened by the effect of stronger concentration of the electric field. In the case of a longer nozzle (case 5), the pressure at the exit,

of the nozzle decreases since the length of the nozzle is longer. Deformation speed is very small and the fluid expands radially for a long time. In this case, the electrostatic force is dominant. In the case of larger radius of the nozzle (case 6), deformation speed is about the same as that in case 1.

It is known experimentally that the fluid configuration is similar to a circular cone. However, this was not observed in the present calculations. It is suspected that this difference is caused by the pressure at the exit of the nozzle and the strength of the electric field. Under the conditions that we used in the calculation, the stress due to surface tension and the pressure at the entrance of the nozzle determined by the surface tension play a dominant part in the deformation of the fluid. Therefore, we expect that the fluid configuration will resemble a cone under conditions of longer nozzle and stronger electric field.

VI. CONCLUSIONS

In this paper, we tried a numerical simulation of a flow ejected from a nozzle by electrostatic force. We used the improved marker and cell method for the motion of the fluid and the charge simulation method for the electric field, respectively. At the free surface, the pressure is determined by the calculation of the surface tension of the fluid and the electrostatic force. Numerical results show reasonable behavior for changes of parameters. Furthermore, the effect of various parameters on fluid deformation can be observed.

Computations were carried out using a HITAC M260D computer. Typical computational time was about 5 hours per case.

REFERENCES

1) Fromm, J.E., Numerical calculation of the fluid dynamics of drop-on demand jets. *IBM. Res. Devel.*, Vol. **28** (1984), pp. 322–333.

2) Katano, Y., Kawamura, T., and Takami, H., Numerical study of drop formation from a capillary jet using a general coordinate system. *Theoretical and Applied Mechanics*, Vol. **34** (University of Tokyo Press, 1986), pp. 3–14.

3) Ebi, Y. and Kawamura, T., Numerical study of droplet formation from liquid jet. *Ricoh Tech. Rep.*, Vol. **5** (1981), pp. 4–11 (in Japanese).

4) Taylor, G., Disintegration of water drops in an electric field. *Proc. Roy. Soc. London. Ser. A*, Vol. **280** (1964), pp. 383–397.

5) Macky, W.A., Some investigations on the deformation and breaking of water drops in strong electric fields. *Proc. Roy. Soc. London, Ser. A*, Vol. **133** (1931), pp. 565–587.

6) Takahashi, D., Takeda, Y., and Takami, H., Numerical simulation of Collision of liquid droplets. *Theoretical and Applied Mechanics*, Vol. **36** (University of Tokyo Press, 1988), pp. 367–380.

7) Kohno, T. and Takuma, T., *Numerical Calculation Method of Electric Field*, 1st ed., Corona Publishing Co. (1980), p. 38 (in Japanese).